Simple, Low-Hysteresis, Foldable, Fabric Pneumatic Artificial Muscle

Nicholas D. Naclerio and Elliot W. Hawkes

***Abstract*—Soft robots offer advantages over rigid robots in adaptability, robustness to uncertainty, and human safety. However, realizing soft actuators for these robots is still a challenge. We present a simple, highly conformable pneumatic artificial muscle made of a thin, single layer of woven, bias-cut fabric. The airtight fabric is adhered together with a flexible adhesive, negating the need for a bladder or sewing. Thus, it is foldable when depressurized and behaves like a McKibben muscle when pressurized, but without the friction of a bladder or braided sheath. Experiments show that the muscle exhibits repeatable, near-linear behavior with less than 1% hysteresis, over an order of magnitude less than that of McKibben muscles. Dynamic testing shows that the muscle responds quickly, even at lengths over 60 cm, contracting in 0.03 s, an order of magnitude quicker than series pouch motors. A fatigue test shows that its life exceeds 100,000 cycles. We also demonstrate that the muscle is well suited for steering tip-extending robots, and actuating folding, deployable structures. Our muscle offers improvements over various existing pneumatic artificial muscles, providing a simple new option for soft robotic actuation that has potential to advance the field.**

***Index Terms*—Soft sensors and actuators, hydraulic/pneumatic actuators, soft robot materials and design.**

I. Introduction

THE PNEUMATIC artificial muscle (PAM) has widespread applications from prosthetics, humanoid robots, mobile robots, continuum robots, and soft robots (see [1] for a review of PAM applications). There are many different PAM designs, most characterized by a soft pneumatic bladder that expands under pressure, causing the actuator to contract [2] or extend [3]. Despite many new PAM designs over the years, the most popular design remains the McKibben muscle; invented by Richard H. Gaylord in 1958 [4] and popularized by physician Joseph L. McKibben soon after [5], [6]. This design uses an airtight bladder surrounded by a braided sleeve of inextensible fibers. As the bladder is pressurized, it expands radially against the sleeve, causing it to contract lengthwise as the angle between the braids decreases [7]. While widely used, the McKibben is limited by its hysteresis, stiffness, fatigue life [8], and non-linear, history-dependent, stress-strain relationship [9].

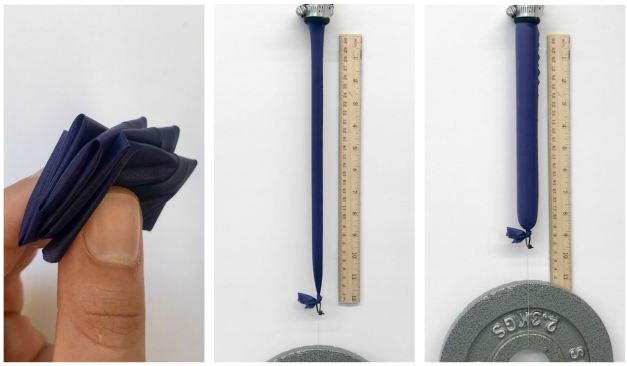

Fig. 1. *Left:* The fPAM in a depressurized, folded state. *Center:* The depressurized, extended state ($\varepsilon = 0$). *Right:* The pressurized, contracted state as it lifts a 2.3 kg mass. The 30 cm long muscle (without compressor or end fixture) has a mass of only 1 g, and a peak contraction of about 30% when unloaded. Ruler is 30.5 cm long for reference.

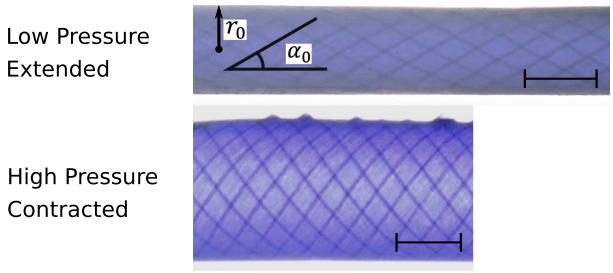

Fig. 2. Backlit photos of the fPAM in a low pressure, extended state (top), and a high pressure, contracted state (bottom). α_0 and r_0 denote initial braid angle and actuator radius, respectively. Scale bars denote 1 cm.

To overcome the limitations of McKibben muscles, we present a simple new PAM made of a single layer of woven, airtight fabric (Fig. 1). The material we use is an airtight, silicone and urethane impregnated, rip-stop nylon fabric, commonly used in camping tents and tarps. The rip-stop pattern is simply a plain weave with thicker, reinforcing strands at regular intervals in both the warp and weft direction (Fig. 2). The key to the operation of the presented fabric PAM (fPAM) is fabric bias. The fabric is relatively inextensible along the major thread lines, but is fairly elastic along the fabric bias at a 45° angle to these threads. This means that a tube of bias-cut fabric will be elastic, while a tube with a straight or cross grain cut will not. As a result, when the tube is pressurized it expands radially while contracting

Manuscript received September 10, 2019; accepted January 26, 2020. Date of publication February 26, 2020; date of current version March 9, 2020. This letter was recommended for publication by Associate Editor Prof. Chen-Hua Yeow and Editor Prof. Kyu-Jin Cho upon evaluation of the reviewers' comments. This work was supported in part by the NSF under Grant 1637446 and in part by NASA Space Technology Research Fellowship. *(Corresponding author: Nicholas Naclerio.)*

The authors are with the Department of Mechanical Engineering, University of California, Santa Barbara, CA 93106 USA (e-mail: nnaclerio@ucsb.edu; ewhawkes@engineering.ucsb.edu).

This letter has supplementary downloadable material available at http://ieeexplore.ieee.org, provided by the authors.

Digital Object Identifier 10.1109/LRA.2020.2976309

lengthwise in a similar fashion as a McKibben muscle. This principle is described in detail in Section II.

While their actuation mechanisms are similar, and both can be classified as braided PAMs [2], the fPAM is distinct from McKibben muscles in that there is no inner-bladder, no stiff outer weave, and most importantly, no friction between the two. Thus, the contributions of this work, and the fPAM more generally, are six desirable attributes, not all found in McKibben muscles or, to the best of our knowledge, in any single PAM: a simple design and fabrication; a predictable, near-linear force-contraction relationship; an absence of hysteresis; a quick response to dynamic inputs; a relatively high fatigue life; and an ability to fold when depressurized, allowing a deployable PAM.

The design of the fPAM builds upon not just the McKibben muscle, but other fabric and film-based PAMs. Several textile PAMs have been made by surrounding an elastic inner tube with a sewn fabric sheath, without taking advantage of an airtight fabric or bias [10], [11]. While knit fabrics have been used in other PAM designs [12], [13], knit fabrics can extend along their stitch directions, meaning that a pressurized knit tube will extend rather than contract. Muscles made of films, or without a bias cut, can only contract like a pouch motor [14], making them geometry dependent. The fPAM mechanism is only dependent on braid angle, not length or diameter. Other actuators have been developed that take advantage of fiber angle by manually programming the angle of fibers wrapped around an elastic inner tube [15], [16].

What follows is first a simple model of fPAM actuation that accurately captures its behavior, followed by a description of its simple fabrication. Next we present experimental results showing: a predictable, near-linear force-contraction relationship with virtually no hysteresis; an improved dynamic response over that of a series pouch motor; a relatively long fatigue life and tube strength; a high degree of repeatable actuation; and sample applications of the fPAM steering a vine robot, and actuating a foldable arm. Finally, we conclude with a discussion of the features and potential applications of the fPAM.

II. Modeling

A. Force vs. Contraction Ratio

The fPAM works in a similar manner to a McKibben muscle, or braided PAM, except that the inner bladder and braid are replaced by an airtight, bias-cut fabric. In both cases, as the muscle is pressurized, it expands radially against the braided fibers, increasing the angle between them as shown in Fig. 2 (see [7] for more details). As the muscle shortens, its volume increases to a maximum point determined by the braid angle. This produces a contraction force that decreases with contraction ratio, ε, where contraction ratio is defined as the decrease in muscle length over its initial length. Given their similarity, we base our modeling of the force-pressure characteristics of the fPAM on previous work for McKibben muscles, modified for the specifics of the fPAM.

The equation for force, F_{ideal}, as a function of contraction ratio for an ideal McKibben muscle, neglecting friction and end effects, has been derived by [7] as

$$\begin{cases} F_{ideal}(\varepsilon) = (\pi r_0^2) P[a(1-\varepsilon)^2 - b], 0 \leqslant \varepsilon \leqslant \varepsilon_{\max} \\ \text{where } a = 3/\tan^2\alpha_0, \text{ and } b = 1/\sin^2\alpha_0. \end{cases} \tag{1}$$

P refers to the internal pressure of the muscle, and r_0 and α_0 refer its initial, depressurized, radius and braid angle respectively, as shown in Fig. 2.

More advanced models for McKibben muscles take into account bladder thickness, elasticity, static friction, and boundary effects at the tip of the actuator. The small regions at the tips of the muscle do not necessarily behave in accordance with the ideal model due to their non-cylindrical shape. Besides tip effects, these issues do not apply for the fPAM because it has no elastic bladder. Here, tip effects are ignored due to their marginal influence on behavior, particularly for long fPAMs.

Instead of directly measuring α_0, it can be determined from a known maximum strain, $\varepsilon_{\max}$, by setting $F_{ideal}(\varepsilon_{\max}) = 0$ and solving for α_0. This gives

$$\alpha_0 = -asin\frac{\sqrt{\varepsilon_{\max}^2 - 2\varepsilon_{\max} + 2/3}}{\varepsilon_{\max} - 1} \tag{2}$$

which can be used to more readily compare the model to experimental results without the need to directly measure α_0, which is challenging to measure accurately.

To build upon the ideal McKibben model and more accurately capture the behavior of the fPAM, we incorporate the pressure-independent elastic force of the muscle, $F_0(\varepsilon)$, produced by the fabric when stretched past its natural length. As such, the force of the fPAM is written as

$$F(\varepsilon) = F_{ideal}(\varepsilon) + F_0(\varepsilon), \tag{3}$$

where $F_0(\varepsilon)$ can be determined experimentally, or approximated by linear elasticity as $2\pi r t E\varepsilon$, or the fPAM circumference, $2\pi r$, times its thickness, t, initial modulus, E, and ε.

B. Maximum Force

In the interest of designing fPAMs with a higher maximum force, we derive an expression for the maximum force an fPAM can exert as a function of its radius and material properties. To find what pressure the fPAM can support, we assume it fails when its hoop stress, σ_θ, equals the ultimate tensile strength, σ_U, of its material:

$$\sigma_U = \sigma_\theta = Pr/t. \tag{4}$$

As the fPAM contracts, σ_θ will be at its maximum when the radius, r, is at its maximum value, $r_{\max}$. The maximum pressure, $P_{\max}$, that the fPAM can support is therefore

$$P_{\max} = t\sigma_U/r_{\max}. \tag{5}$$

Maximum radius, $r_{\max}$, occurs when $F_{ideal} = 0$, while the maximum force, $F_{\max}$, occurs when $\varepsilon = 0$. Ref. [7] found these to be

$$r_{\max} = \sqrt{(2/3)}r_0/\sin\alpha_0 \tag{6}$$

and

$$F_{\max} = \pi r_0^2 P(a-b). \tag{7}$$

Equating (5), (6) and (7) together, we find that the maximum pressure that the fPAM can handle, and the maximum force that it can exert are

$$P_{\max} = \sqrt{(3/2)}t\sigma_U \sin\alpha_0/r_0 \tag{8}$$

and

$$F_{\max} = \sqrt{(3/2)}\pi r_0 t\sigma_U \sin\alpha_0(a-b) \tag{9}$$

respectively. This suggests that for a given material, $F_{\max}$ increases linearly with radius, as opposed to cross sectional area.

III. Fabrication

The fPAM consists of only one main component: a bias-cut, woven fabric tube. The presented prototype was made with a commonly available, nominally 50 μm thick, 30 Denier, silicone and urethane impregnated rip-stop nylon fabric (Seattle Fabrics), often used for camping tents and tarps. This fabric was chosen because it is thin, supple, lightweight, airtight, and can be easily bonded together with a room temperature vulcanizing silicone adhesive (SilPoxy, Reynolds Advanced Materials). This eliminates the need for sewing, and enables the use of lap joints to increase tube compliance and strength. We selected a fabric with a combination of silicone and polyurethane impregnation, because it offers benefits over either material alone. Pure silicone-coated fabrics are not airtight, but pure polyurethane-coated fabrics cannot be bonded with rapid-curing silicone adhesive. Thus this combination is airtight and can be bonded quickly. While the fPAM could also be made of other airtight woven fabrics and manufacturing methods, it will not work with films, nor knit or unbiased fabrics.

fPAM tubes are constructed in a simple manner. First, a strip of fabric is cut along its bias, such that its warp and weft threads are at 45° to the length of the strip (Fig. 3-A). Then, the strip is placed on a work surface, and a thin strip of double-sided tape is placed along its center lengthwise, and attached to the work surface at each end. The tape holds the fabric in place for the following steps (Fig. 3-B). Next, one side of the strip is folded over and adhered to the tape. Then, a thin, continuous bead of silicone adhesive is placed along the length of the edge of the fabric (Fig. 3-C). Finally, the other side of the fabric is folded over and adhered to the silicone adhesive by applying pressure to create a lap joint (Fig. 3-D,E). After waiting for the adhesive to cure, the completed tube can be everted to remove the double-sided tape (Fig. 3-F). The ends of the tube can be attached to pneumatic fittings as desired, or simply tied in a knot to seal them. Measured thickness of the fabric was 71 μm (slightly higher than the nominal value) and 170 μm at the glued lap joints.

For the experiments performed in this study, tubes of various lengths were made with diameters of approximately 22 mm, as measured when $\alpha = 45°$. For secure testing, the fPAMs were attached to simple end-fittings, as shown in the top of Fig. 1. The ends of the tube were placed around 19 mm diameter, 40 mm long aluminum cylinders coated in silicone tape, and secured by hose clamps lined with 6 mm thick neoprene foam. At one end-fitting was attached a 3/8" NPT pneumatic quick-connect fitting for a 1/4" or 1/2" diameter pressure input, and at the other, sealed, end was attached a 1/4"- 20 stud. These end-fittings are not inherent to the fPAM design, but were used to attach them to mechanical testing machines. Otherwise, we simply tied a knot at one end to seal it, as shown in the bottom of Fig. 1 and attached a pneumatic fitting at the other end to pressurize it.

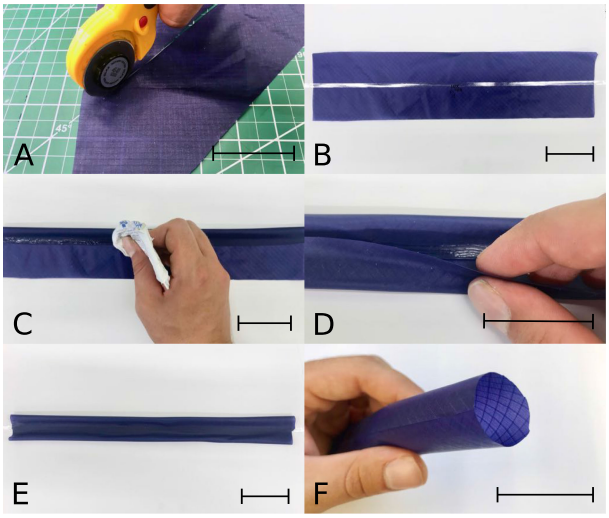

Fig. 3. Series of photos illustrating fPAM fabrication. A) Cut fabric at a 45° bias. B) Lay strip of fabric with double-sided tape down its center. C) Fold top half of fabric over, lengthwise, onto the double-sided tape. Apply thin bead of silicone adhesive along edge of fabric. D) Fold bottom half of fabric over and adhere to applied silicone adhesive. E) Apply pressure and wait for adhesive to cure. F) Evert tube to remove tape and complete manufacturing. Scale bars denote 5 cm.

IV. Experimental Results

A. Force Characterization and Hysteresis

The relationship between force and contraction of the fPAM was examined experimentally by measuring its tensile force output over a range of contraction ratios from 0 to 0.35. Tests were performed with measured body pressures of 0 kPa 34 kPa, 68 kPa, 101 kPa, and 137 kPa, corresponding to approximately 5 psi increments. For each test, a 25 cm long fPAM was attached to a tensile testing machine, with 100 mms^{-1} displacement control by a Twin Rail positioning table, and 20 Hz data recording by an Eaton Lebow 100 lbf load cell. The actuator was connected to a Proportion-Air electronic pressure regulator with 1/4" tubing to maintain a constant internal pressure throughout the test. Three trials were conducted at each pressure, except at 137 kPa where only two trials were conducted before the fPAM slipped out of its end-fitting. The fitting was likely not tightened as much as in later tests.

The results of all tests are shown in Fig. 4 (*left*). The data show that the trials were very repeatable, and there is very little hysteresis. The average hysteresis for the pressurized trails ranged from -0.706% to 0.190% (see Table I). Hysteresis was defined as the difference between the work done by the fPAM during contraction, and the work done on it during extension, divided by the work done in extension. Work was calculated by

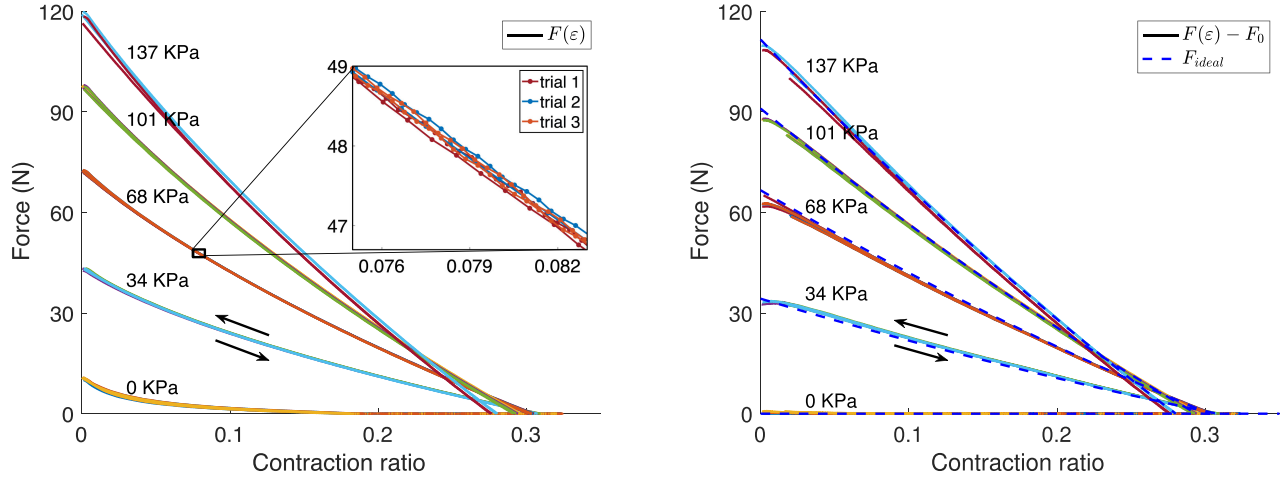

Fig. 4. *Left:* Experimental force vs. contraction ratio ($F(\varepsilon)$) of the fPAM in contraction and extension at various pressures. Contraction ratio is defined as the change in length over extended length. The zoomed plot shows data from the trials conducted at 68 kPa. Note that there is virtually no hysteresis, so the contracting and extending directions appear identical in all trials. Three trials at all pressures (except only two at 137 kPa) are plotted, all falling nearly on top of one another. *Right:* Experimental force vs. contraction ratio ($F(\varepsilon)$) minus the force due to fabric elasticity (F_0) plotted as solid lines. F_0 is approximated as the experimental value of $F(\varepsilon)$ at 0 kPa. Modeled values of F_{ideal} from (1) are plotted as dashed lines (see Section IV-A for more details).

TABLE I
EXPERIMENTAL VALUES FROM FORCE VS. CONTRACTION TEST
(SEE SECTION IV-A)

Pressure (kPa)	0	34	68	101	137
r_0 (mm)		9.5	9.6	9.7	10
α_0 (deg)		33.5	34.1	35.1	36.7
ε_{max}		0.308	0.303	0.294	0.280
Hysteresis (%), avg	13.5	0.190	-0.635	-0.706	-0.529
Hysteresis (%), std	2.03	0.202	0.300	0.103	0.213

numerically integrating force vs. contraction over the range of contraction corresponding to positive force values for each trial. We note that negative hysteresis values are not possible, but are assumed to be within the error of our measurement uncertainty.

Next, we sought to compare the experimental force vs. contraction relationship with our model, (3). To do this, we used experimental $\varepsilon_{\max}$ values found where $F(\varepsilon) = 0$, and calculated α_0 values found by using (2), which was simpler than measuring α_0 directly. Values of r_0 are fitted to the nearest 0.1 mm to minimize error between $F(\varepsilon) - F_0$ and F_{ideal}. These values are recorded in Table I. Using (1) we plotted modeled values of F_{ideal}, as well as the experimental data, $F(\varepsilon)$, minus material elasticity, F_0, in Fig. 4 (*right*). F_0 was approximated as the experimental values of $F(\varepsilon)$ at 0 kPa. Even at 0 kPa, the muscle exerted some force due to its material elasticity in tension. The theoretical model matches the data well, and is near-linear, with an average least-squares linear fit R-squared value of 0.998 across all pressures. Note that the maximum contraction ratios decrease slightly with increasing pressure. This is believed to be caused by fabric elasticity. At higher pressures, the fibers of the fabric strain slightly, expanding the fPAM both radially and lengthwise, as seen by the increasing r_0 values in Table I. As a result, it is slightly longer at its maximum contraction, giving it a slightly lower contraction ratio. This is in contrast

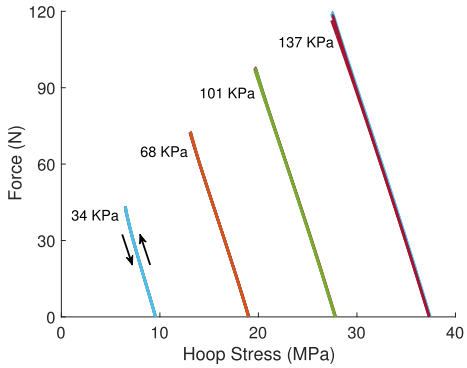

Fig. 5. Experimental actuator force vs. calculated hoop stress, verifying the derivations in Section II-B. Same experimental data as in Fig. 4.

to McKibben muscles, where the contraction ratio increases as pressure increases and internal friction is overcome [9].

In addition, the relationship between hoop stress and tensile force was characterized to verify the derivations in Section II-B. Instead of measuring a few data points of $F_{\max}$, in Fig. 5 we have plotted the data from the tensile test in terms of hoop stress instead of contraction ratio. The results show how hoop stress increases linearly with decreasing force, and that the actuator experiences the most stress when exerting zero force. This means that for a given maximum hoop stress, or ultimate material strength, this characterization must be taken into account, as in (9), to determine the maximum force that the actuator could deliver. For example, limiting the hoop stress to 20 MPa would limit the pressure to about 70 kPa, and maximum force to about 75 N.

B. Dynamic Response

The amplitude frequency response of the fPAM was experimentally compared with that of a series PAM (sPAM) [14].

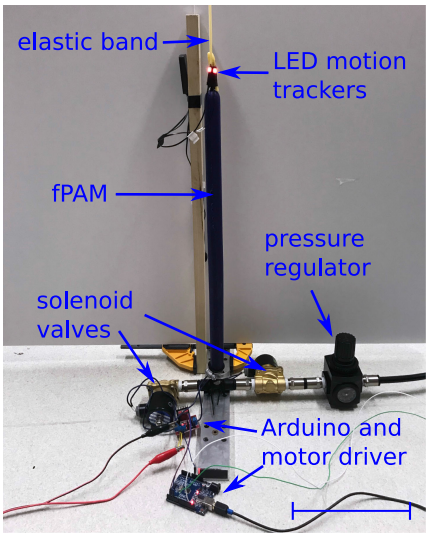

Fig. 6. The motion capture setup used to measure the dynamic response of the fPAM (see Section IV-B). Not shown are the motion capture cameras suspended overhead. Scale bar denotes 20 cm.

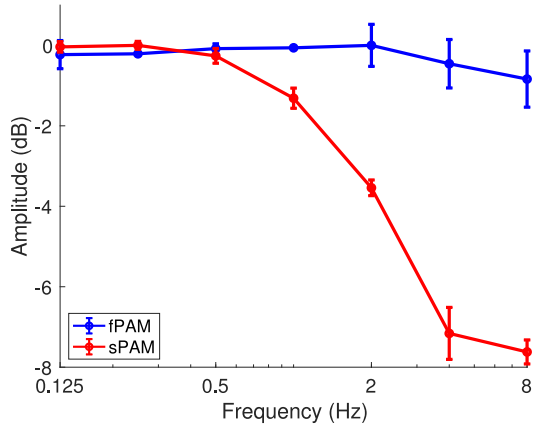

Fig. 7. Frequency response of the fPAM and an sPAM. The average amplitudes and standard deviations of five cycles at each frequency are plotted, normalized by the maximum amplitude. By 8 Hz, the amplitude of the fPAM decreased to about −0.8 dB, or a 10% loss in amplitude. For comparison, the sPAM exceeds this loss by about 0.8 Hz (see Section IV-B).

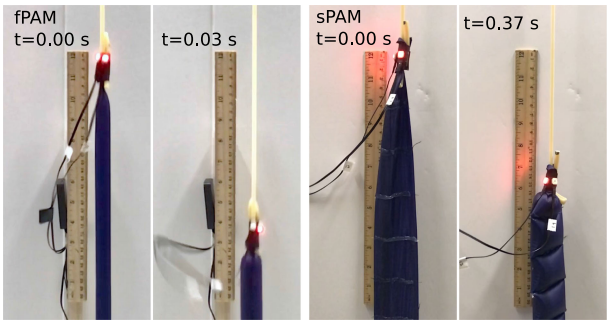

Fig. 8. *Left:* Full contraction of fPAM in 0.03 s. *Right:* For comparison, the sPAM took 0.37 s to contract. Ruler is 30.5 cm long for reference.

We chose an sPAM for comparison, as this is the type of actuator currently used for constant curvature continuum vine robots [17]–[19]. Both actuators were 66 cm long in their extended states. An sPAM such as in [19] was fabricated using the same fabric as the fPAM. A tube was manufactured as described in Section III, except without a bias cut. Pouches were sewn into the tube every 50 mm and sealed with silicone adhesive. A small gap was left in each seam to allow air to flow from one pouch to the next (see Fig. 8).

To test each actuator, its pressurizing end was attached to a metal base, while its free end was tied to a latex tube suspended above it, applying between 2.5 N and 6.5 N of force to restore it to its extended length when depressurized (see Fig. 6). Pressure was modulated as a step function between 0 kPa and 135 kPa by two 1/2" U.S. Solid solenoid valves, one for inflow, and one for outflow, both controlled by an Arduino. To measure position, two LED markers were attached to the free end of the actuator. Their position was recorded by a Phasespace Impulse X2E motion capture system at 960 Hz. Experiments were conducted at 0.125 Hz, 0.25 Hz, 0.5 Hz, 1 Hz, 2 Hz, 4 Hz and 8 Hz for 60 s each.

The results of the experiment are plotted in Fig. 7, showing the average and standard deviation of the end-to-end amplitude of five sequential cycles, normalized by maximum amplitude. By 8 Hz, the amplitude of the fPAM decreased to about −0.8 dB, or a 10% loss in amplitude. For comparison, the sPAM exceeds this loss by about 0.8 Hz. The average contraction and extension times for the fPAM with a stroke length of 170 mm were only 0.033 s and 0.050 s respectively (see Fig. 8). For comparison, the sPAM with a stroke length of 115 mm had average contraction and extension times of 0.37 s and 0.98 s respectively, an order of magnitude slower than the fPAM.

C. Fatigue

To study the durability of the fPAM, a simple fatigue test was conducted. An fPAM with a loaded, depressurized length of 58 mm and 50 g end-fittings as described in Section III was suspended vertically, with one end attached to an air supply, and the other free to hang. Pressure was modulated as a step function between 0 kPa and 100 kPa by two AOMag 1/4" solenoid valves, one for inflow, and one for outflow, controlled by an Arduino. The unloaded fPAM was cycled between contractions and extensions corresponding to a change of ε from 0.13 to 0.23 at 2 Hz for a total of 100,000 cycles. At 1, 100, 1,000, 5,000 and every multiple of 10,000 cycles thereafter, the test was paused and an Omega FLR1202 flow meter was placed inline with the fPAM to measure leakage flow rate. Further, to characterize its performance over time, a single contraction of the fPAM was measured by the Phasespace Impulse X2E motion capture system described in Section IV-B under no load and a load of 4.5 kg. After surviving 100,000 cycles with no measurable leakage or visible damage, the test was terminated. The results in Fig. 9 show that, while there was slight variability between tests, there was no decline in performance over time.

D. Burst Pressure

To determine the burst pressure of the fPAM, we tested a series of devices to failure. Four unrestrained, 8 cm long fPAMs

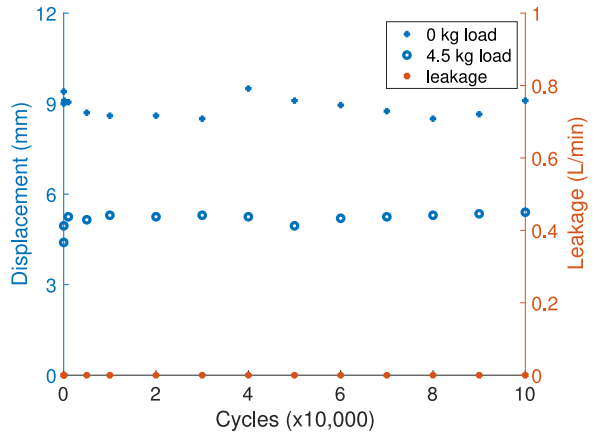

Fig. 9. Contraction and leakage measurements of a 58 mm long fPAM at various cycles during a fatigue test. Pressure was modulated between 0 kPa and 100 kPa at 2 Hz.

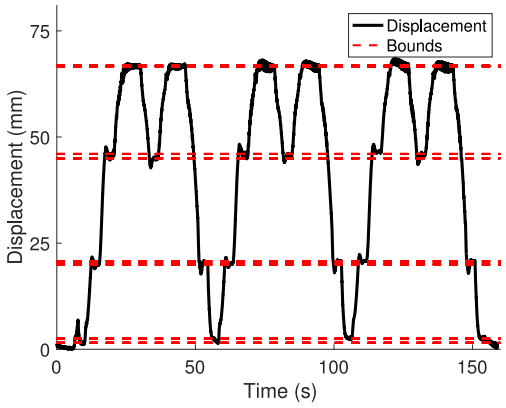

Fig. 10. Recorded displacement of a 275 mm long fPAM under a variable pressure input. Dashed red lines correspond to the maximum and minimum bounds of the displacement for each pressure (see Section IV-E for pressures). The fPAM returns to within 1 mm, or an ε of 0.006, of the same positions, regardless of direction or history. The resistance of the fPAM is low enough to repeatably capture the transient behavior of the pressure regulator. Displacement is zeroed from its initial position.

with the end-fittings described in Section III were subjected to increasing pressure while fully contracted until they burst. The most contracted state is the most susceptible to bursting, since the hoop stress is highest here. In three of the four cases, before the fabric failed, the end-fittings were blown off the fPAM at pressures of 400 kPa, 410 kPa and 430 kPa. In the fourth case, the fabric tore at its connection to the end-fitting and along part of the lap joint at 360 kPa. Taking 360 kPa as a conservative estimate for $P_{\max}$, and a measured $r_{\max}$ of 26 mm, (4) gives the ultimate strength of the tube to be 94 MPa. Using (9), and assuming α_0 and r_0 to be 34° and 10 mm respectively, these results suggest that the maximum force this sized fPAM could exert when fully extended is about 285 N. Note that a higher pressure and force could be achieved in an extended configuration, but the device would burst when contracted as its radius, and thus hoop stress, increases.

E. Repeatability

To demonstrate the repeatability of the fPAM actuation, as well as its history and direction-independence, we inflated the fPAM to a repeating series of pressures under a constant load. We recording its position with the Phasespace Impulse X2E motion capture system described in Section IV-B. A 29 mm diameter, 275 mm long fPAM was suspended vertically, with its top attached to a Proportion-Air electronic pressure regulator with 1/4" tubing. Its bottom was fixed to a 4.5 kg mass, such that the mass would rise as the fPAM was actuated. For three cycles, the pressure was sequentially changed to 0 kPa, 30 kPa, 80 kPa, 130 kPa, 80 kPa, 130 kPa, 30 kPa, and 0 kPa.

Over all three cycles, the fPAM returned to the same four positions, regardless of direction or history, as shown in Fig. 10. The range of displacements that the actuator returned to were 1.0 mm, 0.7 mm, 1.0 mm, and 0.2 mm for pressures of 0 kPa, 30 kPa, 80 kPa and 130 kPa respectively. The maximum range of 1 mm corresponds to a contraction ratio (ε) range of 0.006. Further, the resistance of the fPAM is low enough to repeatably capture the transient response of the electronic pressure regulator.

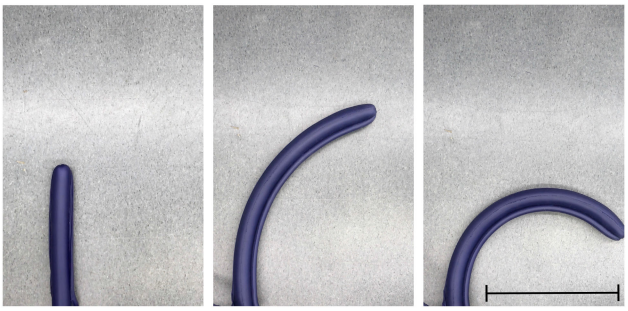

Fig. 11. The fPAM steers a 2 m long vine robot. From left to right, the "vine" robot everts to grow, and then curves while growing as the fPAM attached to its body actuates. See accompanying video. Scale bar denotes 1 m.

F. Steering of Soft Continuum Robot

While the characteristics of the fPAM make it generally suitable to many applications, here we consider the actuation of a soft, tip-extending "vine" robot [20], which can be steered by contracting or lengthening its sides. The vine robot body is composed of an 8 cm diameter, 2 m long tube, identical to an fPAM, but here used as a pneumatic backbone and not used for linear actuation. It is inverted such that when pressurized it pulls new material out its tip as it extends (see [20] for more details). The robot is steered by three 25 mm diameter fPAMs attached along the length of the body, 120° apart for 3D steering. Due to their flexibility, they do not interfere with the robot as it everts, and allow steering during growth. As the left fPAM contracts, the robot curves left, and as the right fPAM contracts it turns right (see Fig. 11).

G. Actuation of Foldable Arm

In a second example application, two antagonistic fPAMs were attached to a simple, folding arm. The arm is made of two foam board segments with a hinge joint between them. The fPAMs are attached to the base of both arm segments

Fig. 12. Antagonistic fPAMs actuate a simple folding arm. From left to right, the left fPAM is contracted, both fPAMs are relaxed, the right fPAM is contracted, and the arm is folded up over the right fPAM. See accompanying video. Scale bar denotes 10 cm.

such that when contracted they can articulate the distal segment right or left (see Fig. 12). Because the fPAMs can flatten when depressurized, the arm can fold back on itself to create a low profile.

V. Discussion

The fPAM features several characteristics that make it well suited for use in soft robotics: a simple and flexible construction, a near-linear relationship between force and contraction, a low-hysteresis actuation cycle, a fast response to dynamic inputs, a durable fatigue life, and an ability to fold when depressurized.

The simplicity and ease of construction of the fPAM design makes it inexpensive and readily accessible to those without specialized tools. Because the fPAM is simply a fabric tube, it is scalable to both arbitrary lengths and diameters, depending on material selection. Our prototype is also very light, weighing only 1 g for a 30 cm long, 25 mm diameter actuator, giving it a maximum force to weight ratio of approximately 12,200:1 at 135 kPa. This is an exaggerated value, though, as it does not include the heavy compressed gas source required to power the actuator. Actuators for higher pressures and greater puncture resistance could be made of stronger fabric and adhesives at the expense of some flexibility. One disadvantage of the fPAM, like McKibben muscles, is that its contraction ratio is limited to about 0.3.

The fPAM exerts a predictable force-contraction relationship that can be represented by a near-linear active component approximated by the behavior of an ideal McKibben muscle, in sum with passive material strain, without the need for more advanced modeling. By using (1), we can predict the maximum force output by an fPAM with different r_0 and α_0 values to more directly compare with existing McKibben muscle data. We find that an fPAM with identical r_0's and α_0's as the McKibben muscles used in [7, Fig. 3] would exert a maximum force of about 80 N and 230 N at a pressure of 100 kPa for α_0's of 20° and 30° respectively. Both of these values lie between the maximum forces of the tests shown in [7, Fig. 3], depending on direction of actuation. However, real McKibben muscles do not follow the ideal McKibben muscle equation due to internal friction caused by bladder-braid and braid-braid interactions. Tests on McKibben muscles in [7, Fig. 3] and [9, Fig. 3] show 10% to 20% hysteresis, which makes these muscles challenging to control [21]. Without this internal friction, the hysteresis of the fPAM is less than 1%, giving it a direction and history independent actuation force.

Because the fPAM is an open fabric tube with no air restrictions, and very low internal friction, air can rapidly flow in and out of it without impedance. This allows the fPAM to have a very fast response to dynamic inputs, operating with a full range of contractions up to about 8 hz. For comparison, we found that the performance of the sPAM drops off after 0.8 hz (Section IV-B). This makes the fPAM better suited for responsive control and teleportation of soft continuum robots, especially at long lengths.

Fatigue life is a critical concern for McKibben-like muscles. Experiments in [8] on unloaded muscles, and [22] on loaded muscles both found that typical McKibben muscles had fatigue lives of less than 18,000 cycles. Ref. [8] also found that fatigue life was severely shortened by an increased contraction ratio. Tests with a full contraction ratio lasted less than 5,000 cycles. Ref. [23] took advantage of this phenomena, and with carefully optimized end-fittings achieved over 12 million cycles, but with a contraction ratio under 6%. The simple fatigue test that we conducted at higher contraction ratios to 100,000 cycles demonstrates that the fPAM is durable despite, and likely because of, its simple construction. Its lack of bladder and external braid reduces the internal interaction forces in the fPAM, potentially extending its fatigue life.

The flexibility of the fPAM makes it well suited for vine robot actuation. Past devices have been actuated by pull tendons or long, series PAMs (sPAMs) (see [14], [17], [18]) due to the their flexibility and ability to deform as the robot everts. The disadvantage of pull tendons on tortuous paths is that friction increases exponentially with robot curvature according to the capstan equation [24]. The disadvantage of sPAMs is that they are slow to respond to pneumatic inputs due to their many air constrictions, especially at long lengths, as shown in Section IV-B. As shown herein, the fPAM is supple like these previous solutions, but not limited by friction or air restrictions.

Interestingly, using the fPAM construction technique for a vine robot body significantly improves its performance in terms of flexibility, durability, and internal friction. Most previous vine robots have been made of low density polyethylene (LDPE) tubes [20], urethane coated nylon [19], or silicone coated fabrics with LDPE bladders [25]. LDPE has limited strength and is susceptible to punctures, limiting the internal pressures and environments that it can operate in. The 150 μm thick urethane coated fabric used in [19] was much stiffer than the fabric used in our prototype, limiting the robot to larger diameters and slow growth. Robots with bladders are similarly limited by stiffness and complexity. The vine body could be made of a bias-cut fabric for increased flexibility and torsional stiffness, or with a straight cut for increased bending stiffness but reduced torsional rigidity [26]. Further, with a bias cut, there is reduced internal friction because the threads glide past each other at a 45° angle instead of dragging directly over each other lengthwise. Ref. [27] found that a bias-cut vine body significantly improved the performance of a device navigating a constrained environment.

Because its body is made only of a single layer of supple fabric, the fPAM can be flattened, folded, and stored when depressurized, lending its use to additional applications unsuitable for McKibben muscles. As shown in the simple example in Section IV-G and Fig. 12, the fPAM can fold flat along with

a folding structure. This opens up the possibility of using it as an actuator in folding, deployable, or origami robots such as [28]–[30]. It could also be routed through a structure like a pull tendon to create complex movements, but without the accumulated friction inherent in tortuous tendon routings. Further, the fPAM is well suited to be used in soft, low-profile, wearable exosuits [13], [31] or shape changing apparel [32].

VI. Conclusion

The fPAM presents a new alternative to traditional PAMs that is simple, flexible, predictable, low-hysteresis, quick-responding, durable, and foldable, based solely on fabric bias. It opens up new opportunities for the actuation of soft robots, deployable and origami structures, exosuits, and active apparel. Future work on the fPAM could include textile and adhesive research to produce sub-millimeter scale actuators as well as extremely high pressure and force macroscale actuators.

Acknowledgment

The authors wish to thank Mario Selvaggio for his assistance building and operating the vine robot.

References

[1] G. Andrikopoulos, G. Nikolakopoulos, and S. Manesis, "A survey on applications of pneumatic artificial muscles," in *Proc. IEEE 19th Mediterranean Conf. Control Autom.*, 2011, pp. 1439–1446.

[2] F. Daerden and D. Lefeber, "Pneumatic artificial muscles: Actuators for robotics and automation," *Eur. J. Mech. Environ. Eng.*, vol. 47, no. 1, pp. 11–21, 2002.

[3] E. W. Hawkes, D. L. Christensen, and A. M. Okamura, "Design and implementation of a 300% strain soft artificial muscle," in *Proc. IEEE Int. Conf. Robot. Autom.*, 2016, pp. 4022–4029.

[4] R. H. Gaylord, "Fluid actuated motor system and stroking device," US Patent 2,844,126, Jul. 22, 1958.

[5] R. Snelson and J. Conry, "Recent advancements in functional arm bracing correlated with orthopedic surgery, for the severely paralyzed upper extremity," *Orthopedic Prosthetic Appl. J.*, vol. 12, pp. 41–48, 1958.

[6] L. Geddes, A. Moore, W. Spencer, and H. Hoff, "Electropneumatic control of the McKibben synthetic muscle," *Orthopedic Prosthetic Appl. J.*, vol. 13, no. 1, pp. 33–36, 1959.

[7] B. Tondu, "Modelling of the McKibben artificial muscle: A review," *J. Intell. Mater. Syst. Struct.*, vol. 23, no. 3, pp. 225–253, 2012.

[8] G. K. Klute and B. Hannaford, "Fatigue characteristics of McKibben artificial muscle actuators," in *Proc. IEEE/RSJ Int. Conf. Intell. Robots Syst.*, 1998, vol. 3, pp. 1776–1781.

[9] C. Chou and B. Hannaford, "Measurement and modeling of McKibben pneumatic artificial muscles," *IEEE Trans. Robot. Autom.*, vol. 12, no. 1, pp. 90–102, Feb. 1996.

[10] G. Belforte, G. Eula, and S. Appendino, "Design and development of innovative textile pneumatic muscles," *J. Textile Inst.*, vol. 103, no. 7, pp. 733–743, 2012.

[11] G. Belforte, G. Eula, A. Ivanov, T. Raparelli, and S. Sirolli, "Study and experimentation of innovative textile pneumatic muscle prototypes," in *Proc. Int. Conf. Robot. Alpe-Adria Danube Region*, 2017, pp. 854–861.

[12] L. Cappello *et al.*, "Exploiting textile mechanical anisotropy for fabric-based pneumatic actuators," *Soft Robot.*, vol. 5, no. 5, pp. 662–674, 2018.

[13] F. Connolly, D. A. Wagner, C. J. Walsh, and K. Bertoldi, "Sew-free anisotropic textile composites for rapid design and manufacturing of soft wearable robots," *Extreme Mech. Lett.*, vol. 27, pp. 52–58, 2019.

[14] R. Niiyama, D. Rus, and S. Kim, "Pouch motors: Printable/inflatable soft actuators for robotics," in *Proc. IEEE Int. Conf. Robot. Autom.*, 2014, pp. 6332–6337.

[15] F. Connolly, C. J. Walsh, and K. Bertoldi, "Automatic design of fiber-reinforced soft actuators for trajectory matching," *Proc. Nat. Acad. Sci.*, vol. 114, no. 1, pp. 51–56, 2017.

[16] F. Connolly, P. Polygerinos, C. J. Walsh, and K. Bertoldi, "Mechanical programming of soft actuators by varying fiber angle," *Soft Robot.*, vol. 2, no. 1, pp. 26–32, 2015.

[17] J. D. Greer, T. K. Morimoto, A. M. Okamura, and E. W. Hawkes, "Series pneumatic artificial muscles (spams) and application to a soft continuum robot," in *Proc. IEEE Int. Conf. Robot. Autom.*, 2017, pp. 5503–5510.

[18] J. D. Greer, T. K. Morimoto, A. M. Okamura, and E. W. Hawkes, "A soft, steerable continuum robot that grows via tip extension," *Soft Robot.*, vol. 6, no. 1, pp. 95–108, 2019.

[19] M. M. Coad *et al.*, "Vine robots: Design, teleoperation, and deployment for navigation and exploration," *IEEE Rob. Autom. Mag.*, 2019, *arXiv:1903.00069*.

[20] E. W. Hawkes, L. H. Blumenschein, J. D. Greer, and A. M. Okamura, "A soft robot that navigates its environment through growth," *Sci. Robot.*, vol. 2, no. 8, 2017 Art. no. eaan3028.

[21] T.-J. Yeh, M.-J. Wu, T.-J. Lu, F.-K. Wu, and C.-R. Huang, "Control of mckibben pneumatic muscles for a power-assist, lower-limb orthosis," *Mechatronics*, vol. 20, no. 6, pp. 686–697, 2010.

[22] D. A. Kingsley and R. D. Quinn, "Fatigue life and frequency response of braided pneumatic actuators," in *Proc. IEEE Int. Conf. Robot. Autom.*, 2002, vol. 3, pp. 2830–2835.

[23] B. K. Woods, M. F. Gentry, C. S. Kothera, and N. M. Wereley, "Fatigue life testing of swaged pneumatic artificial muscles as actuators for aerospace applications," *J. Intell. Mater. Syst. Struct.*, vol. 23, no. 3, pp. 327–343, 2012.

[24] J. W. Hearle and W. E. Morton, *Physical Properties of Textile Fibres*. New York, NY, USA: Elsevier, 2008.

[25] N. D. Naclerio, C. M. Hubicki, Y. O. Aydin, D. I. Goldman, and E. W. Hawkes, "Soft robotic burrowing device with tip-extension and granular fluidization," in *Proc. IEEE/RSJ Int. Conf. Intell. Robots Syst.*, 2018, pp. 5918–5923.

[26] P. Potluri, A. Manan, M. Francke, and R. Day, "Flexural and torsional behaviour of biaxial and triaxial braided composite structures," *Compos. Struct.*, vol. 75, no. 1–4, pp. 377–386, 2006.

[27] D. A. Haggerty, N. D. Naclerio, and E. W. Hawkes, "Characterizing environmental interactions for soft growing robots," in *Proc. IEEE/RSJ Int. Conf. Intell. Robots Syst.*, 2019, pp. 3335–3342.

[28] S. Pellegrino, *Deployable Structures*. Berlin, Germany: Springer, 2014, vol. 412.

[29] S. Miyashita, S. Guitron, M. Ludersdorfer, C. R. Sung, and D. Rus, "An untethered miniature origami robot that self-folds, walks, swims, and degrades," in *Proc. IEEE Int. Conf. Robot. Autom.*, 2015, pp. 1490–1496.

[30] E. V. Hoff, D. Jeong, and K. Lee, "Origamibot-i: A thread-actuated origami robot for manipulation and locomotion," in *Proc. IEEE/RSJ Int. Conf. Intell. Robots Syst.*, 2014, pp. 1421–1426.

[31] M. Wehner *et al.*, "A lightweight soft exosuit for gait assistance," in *Proc. IEEE Int. Conf. Robot. Autom.*, 2013, pp. 3362–3369.

[32] L. Perovich, P. Mothersill, and J. B. Farah, "Awakened apparel: Embedded soft actuators for expressive fashion and functional garments," in *Proc. 8th Int. Conf. Tangible, Embedded Embodied Interact.*, 2014, pp. 77–80.